Vibration Suppression Based On Adaptive Feedforward Control With Infinite Impulse Response Filter

Shiying Zhou and Masayoshi Tomizuka

Mechanical Engineering

University of California, Berkeley

December 2015

Abstract

This report presents adaptive feedforward control for vibration suppression based on an infinite impulse response (IIR) filter structure. The vibration signal and the output signal are available for the algorithm to adaptively update the parameters of the vibration transmission path (VTP) dynamics. Two designs for parameter adaptation are proposed. They provide different methods to get the necessary signals for parameter adaptation of the IIR filter which is different from the conventional finite impulse response (FIR) filter adaptation design. Performance of the proposed designs is compared with the conventional Filtered-x Least Mean Square (FxLMS) method on a hard disk drive (HDD) benchmark problem. The simulation results show that the proposed designs have smaller 3σ value and peak to peak value at steady state.

This work was supported by the Computer Mechanics Laboratory (CML) in the Department of Mechanical Engineering, University of California, Berkeley.

This work has been presented at the 2015 Dynamic Systems and Control (DSC) Conference in Columbus,Ohio, October 2015 [Zhou et al. (2015)].

1 INTRODUCTION

Nowadays, HDDs have been used extensively as cost-effective and reliable solutions for data storage. In addition to its usual utilization in desktops, an increasing number of portable electronic devices such as laptops and tablets are using HDDs to store digital data. In these applications, HDDs are usually subject to external vibrations and shocks from surroundings, such as audio speakers nearby and shocks from human activities. These external disturbances are generally concentrated at low frequencies ($0 - 2000Hz$). They will increase the position error signal (PES), i.e. deviation of the read/write head from the desired track center and result in a large track mis-registration (TMR), namely, 3σ, which is defined as three times of the standard deviation of the PES. On the other hand, the density of data stored on the magnetic disk is increasing drastically and the large tracks per inch (TPI) requires better vibration-suppression capability of the HDD control system.

External vibration rejection methods include feedback and feedforward control. The conventional feedback methods use loop shaping to shape the sensitivity function of the system [4, 11, 17]. One limitation of feedback based methods is the trade-off between bandwidth and stability margin. The increase of the bandwidth is often accompanied by the decrease in stability margin. Another limitation is due to the waterbed effect in linear system by Bode's Integral Theorem [15], i.e. the sensitivity suppression at some frequency regions will inevitably lead to sensitivity amplification at other regions. So the compromise between vibration rejection and unwanted high frequency amplification is an issue in conventional feedback design methods.

Due to the aforementioned limitations in conventional linear feedback design, feedforward design methods are investigated in this report. Generally, the disturbances information is necessary for the feedforward control design. In some cases, the models of the disturbances are known in advance and can be directly employed for vibration suppression, as addressed in [3, 19]. In other cases, the disturbances entering the servo system can be measured by properly installed sensors. Then by offline or online design of additional filters, the feedforward signal can be generated and injected into the loop to cancel the disturbances. However, the disturbances nature and the HDD dynamics are subject to change. Different units of HDDs will cause system variations and so do using and aging of the HDDs.Therefore, it will be advantageous to make the vibration compensation adaptive.

Among different adaptive feedforward control methods for vibration suppression, the Filtered-x Least Mean Square (FxLMS) method [2] has been widely used in HDD vibration suppression where it cancels the vibration effect with measured vibration signal by utilizing the output from an adaptive finite impulse response (FIR) filter. There are some benefits for using adaptive FIR filter in feed-forward compensation. First, the dynamics of an FIR filter is straightforward that the output is only determined by the input signal which means the signals needed for the adaptation can be obtained effortlessly; Second, due to simplicity of the FIR dynamics, no stability issue needs to be considered during the adaptation; Finally, simple gradient algorithm like least mean square (LMS) [2] can be applied to update the FIR coefficients with a fast and well-understood convergence behavior for a simple unknown VTP dynamics [10]. For example, gradient algorithms were used to adapt an FIR filter online to approximate the vibration transmission path (VTP) dynamics in HDD [16, 18].

Compared to the adaptive FIR, the IIR-based adaptive feedforward control has two benefits:

1. It provides more accurate approximation to the actual VTP dynamics which has an IIR structure;
2. It is more efficient that it can approximate the unknown dynamics with fewer parameters than an FIR filter.

However, there are also some drawbacks that hinder the application of adaptive IIR filter:

1. Since IIR filters represent the coupling relationship between input and output that the signals needed for the parameter adaptation can not be obtained without proper block diagram modification for feasible implementation with stable and converging behavior;
2. The poles of the IIR filter may go beyond the unit circle [13] during adaptation which will cause instability;
3. The convergence speed for adaptive IIR is generally not so desirable.

As a result, even though the active noise control (ANC) using adaptive IIR has been investigated since at least the mid-1980s [7] and applications using adaptive IIR for noise cancellation can be found in many literatures [6, 10], there are still some questions that are not answered explicitly.

1. the general algorithm used for adaptive IIR is recursive least square (RLS) in output-error(OE) form which is bimodal [10];
2. the stability of the OE form algorithm is often hard to prove and guarantee [1].

The alternative is to use equation-error(EE) form RLS algorithm, but it is much more difficult because of the need to generate estimates of the desired signals [8] and the error convergence of the algorithm was not proved rigorously, either. Moreover, the application of an adaptive IIR for feed-forward compensation in HDD is hardly found according to the best knowledge of the author. The IIR filter is designed, but in offline mode ([18]).

Concerning the above difficulties with adaptive IIR, this report focuses on an adaptive feed-forward control for vibration suppression based on an IIR filter structure and its application in HDDs. Two designs are proposed to extract the necessary signals for parameter adaptation with additional filtering to guarantee the error convergence. Stability of the adaptive IIR is handled by projecting the poles into the unit circle [5] with details in Section 3.2. The RLS method is used for the parameter adaptation with additional signal normalization and deadzone handling for algorithm stability and robustness. Besides, the resulting adaptation algorithm's error convergence is rigorously proved. The convergence speed of the proposed designs are not studied. But the relative IIR-RLS and FIR-LMS convergence speed is studied in [10] and the author found comparable rate of convergence between these two algorithms. It is also seen in the simulation that the proposed designs achieve superior compensation performance at steady state and faster convergence of error

for complicated VTP dynamics. It is also robust to the color noise as long as the bound for the noise is known and is not excessively large. In addition, it can be integrated to the existing baseline control structure easily.

The rest of the report is organized as follows. The problem and the two proposed designs are introduced in Section 2. The parameter adaptation algorithm (PAA) and stability analysis for error convergence are given in Section 3 with additional discussion for stability, signal normalization and robustness. The simulation results of both designs with one case of VTP dynamics are shown in Section 4. Section 5 summaries the report.

2 THE PROBLEM AND PROPOSED DESIGNS

Design 1: Throughout the report, the vibration suppression in the track-following problem of HDD will be focused. The block diagram of the first proposed design is shown in Fig. 1 . The signals in the block diagram are defined as follows:

- $v(k)$: the vibration signal measured by the vibration sensor
- $G_{vtf}(z^{-1})$: the dynamics of the VTP, which may be expressed as $\frac{B(z^{-1})}{A(z^{-1})}$ if no delay is assumed
- $\frac{\hat{B}(z^{-1})}{\hat{A}(z^{-1})}$: the adaptive system updated by the PAA
- $\hat{S}(z^{-1})$: the estimate of the secondary path dynamics, which is the dynamics between the two '=' marks
- $P(z^{-1})$, $C(z^{-1})$: the full order plant and the baseline feedback controller for the system
- $v'(k)$, $e_f(k)$, $y_f(k)$: the signals used for the PAA

The secondary path is used to align the time step mismatch between the vibration signal and the position error signal (PES), an offline identification for the secondary path dynamics is necessary.

The well formulated open-source HDD benchmark simulation package [9] is used in the simulation for verification. A practical model for HDD plants can be of orders higher than twenty and with several high frequency resonances, as shown in Fig. 3. Due to the complexity of the full order model, significant resonances are attenuated by notch filters and the full order model is reduced to a second order system for the baseline controller design. The baseline feedback controller $G_c(s)$ is a Proportional-Integral-Derivative (PID) controller cascaded with three notch filters. The baseline closed loop system has a gain margin of $5.81dB$, a phase margin of 47.7 degree and a bandwidth of about $1000Hz$.

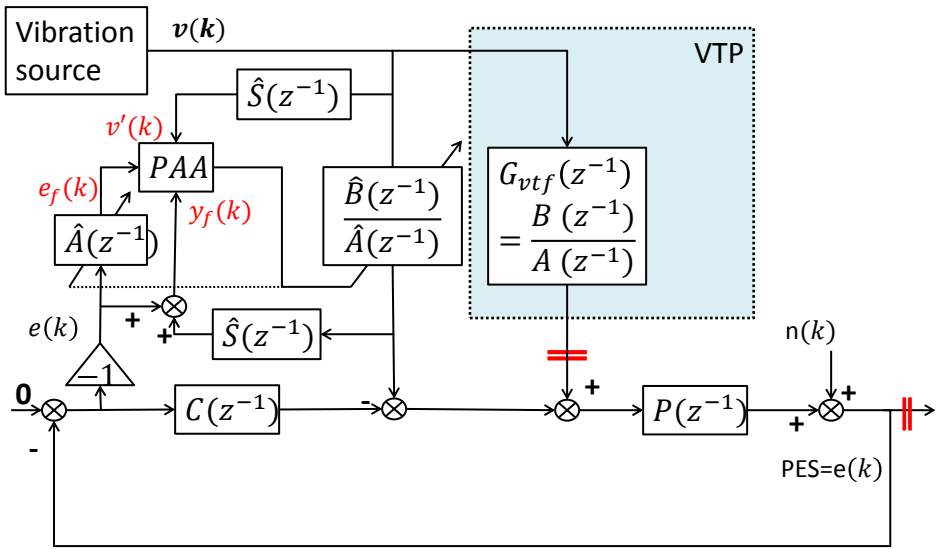

Figure 1: PROPOSED BLOCK DIAGRAM 1

From Fig. 1 , it can be seen that the external vibration goes through the VTP and enters the HDD servo loop. Thus the vibration signal $v(k)$ cannot be used directly to cancel the vibration by the feedforward method. An adaptive IIR filter is added to filter the sensor signal before it is used for the feedforward control.The proposed design focuses on the vibration suppression at low frequencies (about $0Hz$ to $1500Hz$) under the following assumptions:

A1. After proper feedback design, all the errors present at output PES come from the external vibration $v(k)$;

A2. $S(e^{-j\omega}) = \frac{P(e^{-j\omega})}{1+P(e^{-j\omega})C(e^{-j\omega})} \approx \hat{S}(e^{-j\omega})$ for $\omega/(2\pi T_s) \in [0, 1500Hz]$. In the case where the sensor signal has higher energy at other frequencies, the algorithm can still work as long as $S(z^{-1}) \approx \hat{S}(z^{-1})$ in that frequency range.

Design 2: Since the plant model is assumed to be available when the controller is designed, Design 2 as shown in Fig. 2 is also proposed when secondary path dynamics in Design 1 is difficult to estimate. The notations in Fig. 2 are similar to those in Fig. 1 and the black solid lines marked with number 1 are replaced by the blue dash lines marked with number 2 to obtain signal $e_f(k)$. If $P(z^{-1})\hat{P}n^{-1} \approx z^{-d}$ in the frequency range where the vibration concentrates, the estimate of the disturbance can be obtained as $\hat{d}(k-d)$. After filtering $\hat{d}(k-d)$ through Q filter, which includes lowpass or bandpass filters to constrain the signal in the vibration frequency range, the necessary signals for the adaptation can be obtained from this structure.

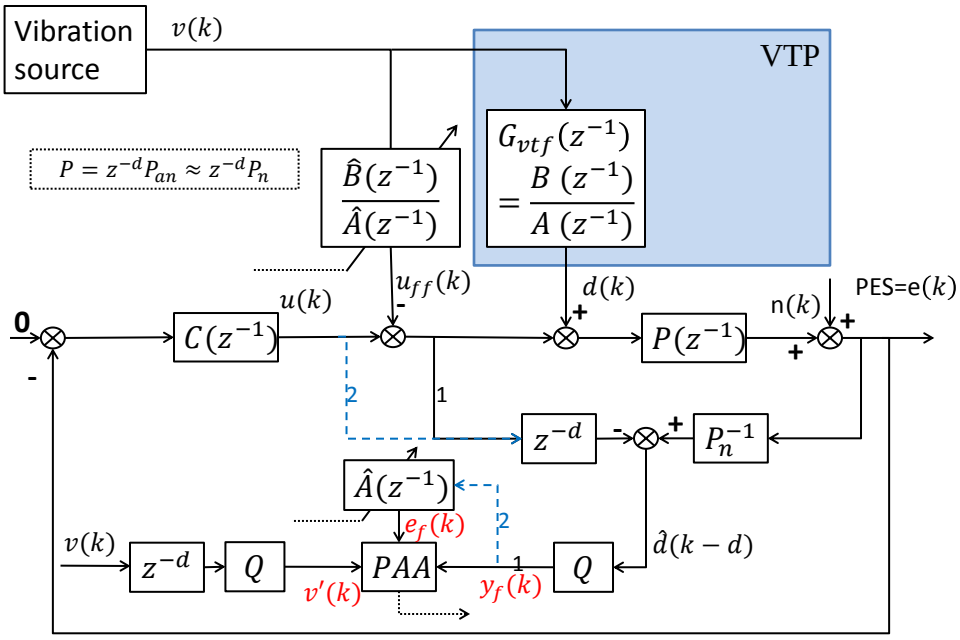

Figure 2: PROPOSED BLOCK DIAGRAM 2

3 ADAPTIVE FEEDFORWARD ALGORITHM

3.1 The Parameter Adaptation Algorithm

The PAAs for Design 1 and 2 are the same. Therefore, only Design 1 will be used for derivation. The proposed block diagram for Design 1 is shown in Fig. 1. It can be rearranged as shown in Fig. 4. In the equivalent block diagram, the VTP dynamics and the adaptive filter are in parallel structure. If the secondary path dynamics is neglected, the structure will approximate the system identification configuration.

Since the noise term $n(k)$ in Fig. 1 and Fig. 4 do not affect the stability, they are dropped in the development of equations in the following. The dynamic path from $v(k)$ to $e(k)$ in Fig. 4 yields

$$P(z^{-1})\Big(\big(\frac{B(z^{-1})}{A(z^{-1})} - \frac{\hat{B}(z^{-1})}{\hat{A}(z^{-1})}\big)v(k) - C(z^{-1})e(k)\Big) = e(k) \tag{1}$$

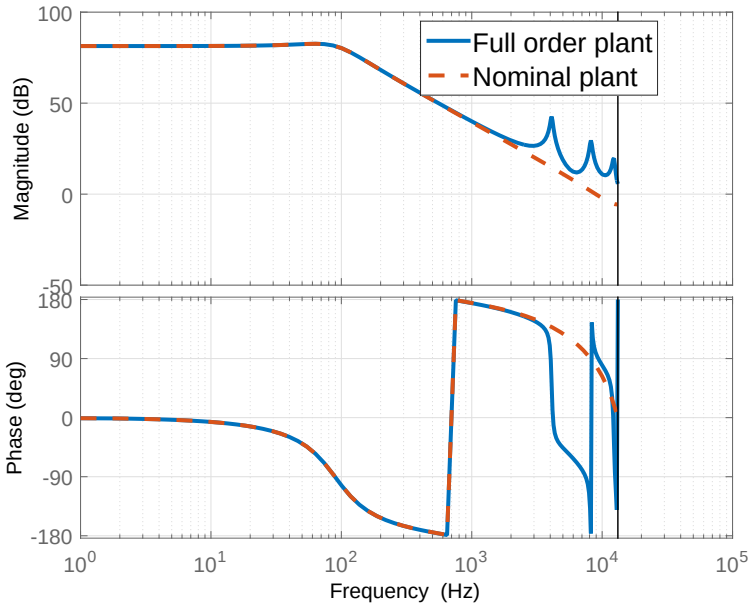

Figure 3: BODE PLOT OF THE FULL ORDER AND NOMINAL HDD PLANT

Multiplying $\frac{1}{1+P(z^{-1})C(z^{-1})}$ to the both sides of Eq. (1) ,

$$\frac{P(z^{-1})}{1+P(z^{-1})C(z^{-1})}\Big(\frac{B(z^{-1})}{A(z^{-1})}-\frac{\hat{B}(z^{-1})}{\hat{A}(z^{-1})}\Big)v(k)=e(k) \tag{2}$$

Denoting $S(z^{-1}) \triangleq \frac{P(z^{-1})}{1+P(z^{-1})C(z^{-1})}$ and $v'(k) \triangleq S(z^{-1})v(k)$, Eq. (2) leads to

$$\frac{B(z^{-1})}{A(z^{-1})}v'(k)=S(z^{-1})\frac{\hat{B}(z^{-1})}{\hat{A}(z^{-1})}v(k)+e(k) \tag{3}$$

Denoting $y_f(k) \triangleq S(z^{-1})\frac{\hat{B}(z^{-1})}{\hat{A}(z^{-1})}v(k)+e(k)$, Eq. (3) yields

$$\frac{B(z^{-1})}{A(z^{-1})}v'(k)=y_f(k) \tag{4}$$

Under Assumption A1 in Section 2, $S(z^{-1})$ can be replaced by $\hat{S}(z^{-1})$ without losing the accuracy for adaptation in the low frequency range. Thus far the generation of $v'(k)$ and $y_f(k)$ in the bottom portion of Fig. 4 has been explained. Next, it will be shown that $e_f(k)$ in Fig. 4 can be used in PAA to guarantee the stability of the algorithm.

$e_f(k)$ in Fig. 4 is represented as

$$\begin{aligned} e_f(k) &= \hat{A}(z^{-1},k-1)e(k) \\ &= \hat{A}(z^{-1},k-1)S(z^{-1})\Big(\frac{B(z^{-1})}{A(z^{-1})}v(k)-\frac{\hat{B}(z^{-1},k-1)}{\hat{A}(z^{-1},k-1)}v(k)\Big) \end{aligned} \tag{5}$$

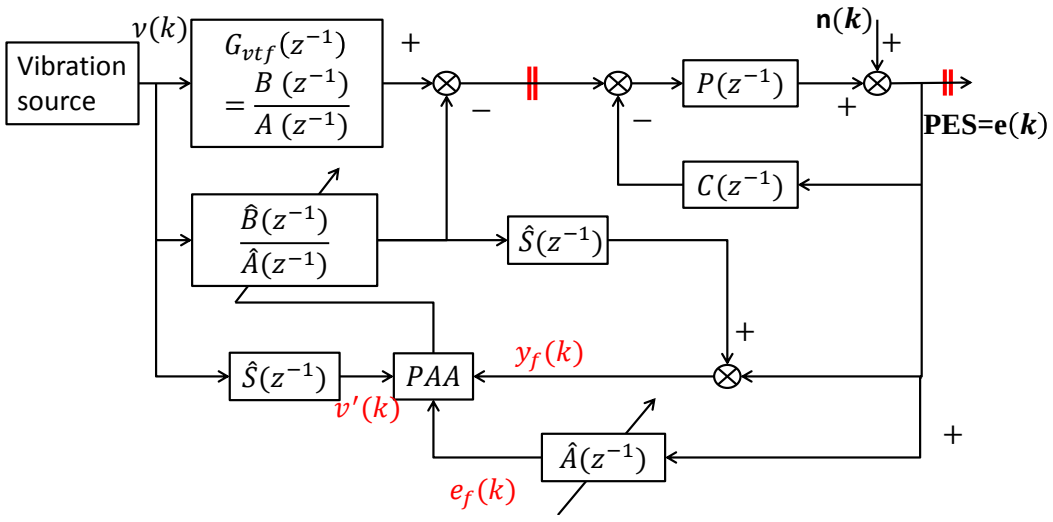

Figure 4: EQUIVALENT BLOCK DIAGRAM OF THE ONE IN FIGURE. 1

If $\hat{A}(z^{-1})$ and $\hat{B}(z^{-1})$'s coefficients were updating slowly[1] with respect to time, the order of operations by $S(z^{-1})$, $\hat{A}(z^{-1})$ and $\hat{B}(z^{-1})$ on the signal $\nu(k)$ can be commuted [6]. Thus,

$$\begin{aligned} e_f(k) &= \hat{A}(z^{-1}, k-1)\frac{B(z^{-1})}{A(z^{-1})}v'(k) - \hat{B}(z^{-1}, k-1)v'(k) \\ &= \hat{A}(z^{-1}, k-1)y_f(k) - \hat{B}(z^{-1}, k-1)v'(k) \end{aligned} \tag{6}$$

Denoting the regressor $\phi_f(k-1) \triangleq [-y_f(k-1), \quad ... \quad -y_f(k-n)\,, v'(k)\,, \quad ... \quad v'(k-m)]^T$, the measurement vector $\hat{\theta}(k) \triangleq \left[\hat{a}_1(k), \quad ... \quad \hat{a}_n(k)\,, \hat{b}_0(k)\,, \quad ... \quad \hat{b}_m(k)\right]^T$ and assuming zero delay of the VTP dynamics, Eq. (6) can be written as

$$e_f(k) = y_f(k) - \hat{\theta}(k-1)^T\phi_f(k-1) \tag{7}$$

With the above input, output and error signals, the RLS parameter adaptation algorithm becomes the following [12]:

$$\hat{\theta}(k) = \hat{\theta}(k-1) + \frac{F(k-1)\phi_f(k-1)e_f(k)}{1+\phi_f^T(k-1)F(k-1)\phi_f(k-1)} \tag{8}$$

$$e_f(k) = y_f(k) - \hat{\theta}^T(k-1)\phi_f(k-1) \tag{9}$$

$$F(k) = \frac{1}{\lambda(k-1)}[F(k-1) - \frac{F(k-1)\phi_f(k-1)\phi_f^T(k-1)F(k-1)}{\lambda(k-1)+\phi_f^T(k-1)F(k-1)\phi_f(k-1)}] \tag{10}$$

$$\lambda(k) = 1 - 0.05 \times 0.995^k \tag{11}$$

[1]It can be shown that $S\hat{B}v(k) - \hat{B}Sv(k) = \sum_{j=0}^{n_s} s_j\{\sum_{i=0}^{n_B}(b_i(k-j) - b_i(k))\nu(k-j-i)\}$, so if coefficients of B is changing slowly with respect to step which is the order of B, assumption is met.

The forgetting factor $\lambda(k)$ is designed to increase from 0.95 to 1 in Eq. (11) to accelerate the convergence rate [12].

3.2 Stability Analysis

By using the PAA of Eqs. (8)-(11), the error $e_f^*(k) = e_f(k)/(1 + \phi_f^T(k-1)F(k-1)\phi_f(k-1))$ can be proved to converge to zero as the adaptation is performed in the frequency range where $S(z^{-1}) = \hat{S}(z^{-1})$. However, the noise, which has been neglected in equations in Section 3.1, is generally not white and the adaptive IIR will be an underestimate of the true unknown dynamics which has higher order and mismatch between $S(z^{-1})$ and $\hat{S}(z^{-1})$ exists. Thus the parameters will not converge to the true values. The goal, however, is vibration suppression and the parameter convergence will not influence the performance.

The key steps in the stability analysis of the PAA by hyperstability [12] are outlined in the followings.

- **Error Equation:**
  Denoting $\tilde{\theta}(k) \triangleq \hat{\theta}(k) - \theta(k)$ and combining this with Eq. (7),

  $$e_f^*(k) = -\tilde{\theta}(k)^T \phi_f(k-1) \tag{12}$$

  Subtracting θ from Eq. (8),

  $$\tilde{\theta}(k) = \tilde{\theta}(k-1) + F(k-1)\phi_f(k-1)e_f^*(k) \tag{13}$$

- **Equivalent feedback loop:**
  Combining Eq. (12) and Eq. (13), the equivalent feedback loop for the adaptive system can be constructed as shown in Fig. 5 where $\lambda^* = \max_k \lambda(k)$. The nonlinear block NL in Fig. 5 can be shown to be passive and satisfies the Popov inequality [12]. The feedback loop formed by the linear strictly positive real (SPR) block L2 and NL is still passive and satisfies Popov inequality. L1 is a parallel connection of the positive unity constant and the constant $\lambda^*/2 < 1$ and it is passive. Thus, the overall adaptive system is asymptotically hyperstable. As a result [12], $\lim_{k\to 0} e_f^*(k) = 0$.

  The actual PES is related to $e_f^*(k)$ by $e_f(k) = \hat{A}(z^{-1}, k-1)e(k)$ and $e_f^*(k) = e_f(k)/(1 + \phi_f^T(k-1)F(k-1)\phi_f(k-1))$. Therefore, $e_f^*(k)$ is a moving average of the PES normalized by some bounded signal $\phi_f(k)$. When the adaptive parameters converge to the steady state value, PES will also converge to zero as $e_f^*(k)$ converges to zero.

Additional considerations:

For implementation of the algorithm, some additional considerations should be given for practical concerns:

- **Stability of Adaptive IIR** [5]:
  The adaptive IIR filter becomes unstable when the poles shift outside the unit circle during adaptation. The poles can be either monitored by their geometric position to the unit circle or different parameterization of the adaptive IIR filters [5,13]. In this work, the stability of the adaptive IIR is checked at every iteration. Assume the adaptive IIR can be parameterized with stable and unstable parts: $G(z^{-1}) = \frac{B(z^{-1})}{A^+(z^{-1})A^-(z^{-1})}$ and $A^-(z^{-1}) = 1 + a_1 z^{-1} + \ldots + a_{nu} z^{-nu}$ contains all poles outside unit circle. The stability is preserved by projecting the unstable poles into the unit circle: $A^-_{proj}(z) = z^{-nu} + a_1 z^{-nu+1} + \ldots + a_{nu}$. To apply this idea, $\hat{A}(z^{-1}, k)$ is factored to the product $\hat{A}^+(z^{-1}, k)\hat{A}^-(z^{-1}, k)$ and replaced by $\hat{A}^+(z^{-1}, k)\hat{A}^-_{proj}(z^{-1}, k)$. This adds a fair amount of real time computation, in particular, if the order of $A(z^{-1})$ is high.

- **Signal Normalization:**
  In order to prevent instability when the input and output signal grow unbounded, the normalized signals $\phi_{fn}(k)$ and $e_{fn}(k)$ are used in the implementation instead of $\phi_f(k)$ and $e_f(k)$. A standard method of signal normalization is [[1]] :

$$m(k) = g_1 m(k-1) + g_2 \max\{1, \|\phi_f(k)\|\} \tag{14}$$

$$\phi_{fn}(k) = \phi_f(k)/m(k); e_{fn}(k) = e_f(k)/m(k) \tag{15}$$

  where $g_1 = 0.9, g_2 = 1$ is used.

- **Robustness:** [12]
  When noise and/or modeling error exist(s), the stability of the algorithm may be lost. Thus a deadzone is added for the robustness concern. Instead of $e_f(k)$, $D[e_f(k)]$ will be used in implementation:

$$D[e_f(k)] = \begin{cases} 0 & \text{if } |e_f(k)| < \delta \\ e_f(k) & \text{if } |e_f(k)| \geq \delta \end{cases} \tag{16}$$

  where δ is a bound for the uncertainties including noise. In the simulation, δ is chosen as the largest absolute value of noise magnitude which is assumed known. Obviously, the magnitude of the noise should not be excessively large.

  With the inclusion of signal normalization and deadzone handling to the PAA algorithm in Eqs.(8)-(11), the final PAA algorithm for implementation in the simulation becomes the following:

$$\hat{\theta}(k) = \hat{\theta}(k-1) + \frac{F(k-1)\phi_{fn}(k-1)e_{fnd}(k)}{1 + \phi^T_{fn}(k-1)F(k-1)\phi_{fn}(k-1)} \tag{17}$$

$$e_f(k) = y_f(k) - \hat{\theta}^T(k-1)\phi_f(k-1) \tag{18}$$

$$F(k) = \frac{1}{\lambda(k-1)}[F(k-1) - \frac{F(k-1)\phi_f(k-1)\phi^T_f(k-1)F(k-1)}{\lambda(k-1) + \phi^T_f(k-1)F(k-1)\phi_f(k-1)}] \tag{19}$$

$$\lambda(k) = 1 - 0.05 \times 0.995^k \tag{20}$$

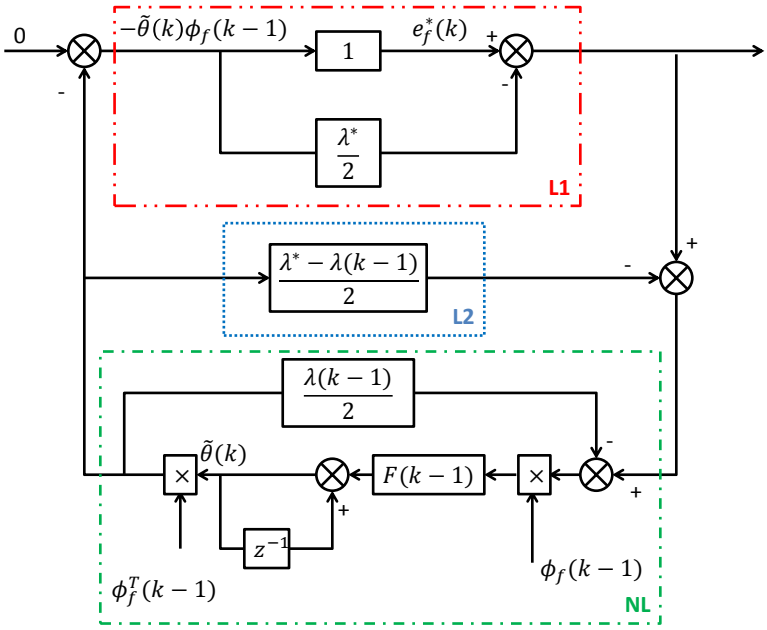

Figure 5: EQUIVALENT FEEDBACK LOOP OF THE ADAPTIVE SYSTEM

where

$$e_{fnd}(k) = \begin{cases} 0 & \text{if } |e_f(k)| < \delta \\ e_{fn}(k) & \text{if } |e_f(k)| \geq \delta \end{cases} \tag{21}$$

4 SIMULATION RESULTS

The proposed Design 1 and 2 were implemented and compared with the FxLMS algorithm on the HDD benchmark simulation package [9]. External vibration is measurable and colored output noise is injected. The sampling time is $3.7879 \times 10^{-5} sec$. The secondary path dynamics $S(z^{-1})$ was estimated using the System ID toolbox in MATLAB. The bode plots of $\hat{S}(z^{-1})$ and $S(z^{-1})$ are shown in Fig. 6. From the figure, it can be seen that the mismatch becomes large above about $2000Hz$. Signals used for the PAA are filtered by low pass filters with cutoff frequency at $3000Hz$. In HDD, the VTP dynamics generally includes mechanics based spindle actuation and some external chassis mechanics. The solid line in Fig.8 is used as the VTP dynamics in the simulation. Other simulation parameters are shown in Table 1.

Four control approaches have been compared:

Table 1: SIMULATION PARAMETERS

–	d	m	n
VTP dynamics	0	4	4
Adaptive IIR	0	3	3
Adaptive FIR	7 unknowns	$\mu = 2 \times 10^{-5}$	

Table 2: SIMULATION RESULTS

–	BS	BC+FxLMS	BC+Design 1	BC+Design 2
3σ	4.1	1.71	0.34	0.42
Peak to peak	10.6	4.15	0.87	1.14

1. baseline control (BC);
2. BC plus FxLMS;
3. BC plus the proposed design 1;
4. BC plus the proposed design 2.

The PES power spectrum and time response of these cases are shown in Fig. 7 and the peak-to-peak value and 3σ value are listed in Table 2. It can be seen that both proposed designs achieve better performance than FxLMS method and the transient is much faster. The steady state Bode plots of the adaptive IIR and the VTP dynamics are shown Fig. 8. It can be seen that the adaptive IIR does not converge exactly to the actual dynamics. This is due to the adaptive IIR being an underestimate of the actual dynamics and model mismatches between $S(z^{-1})$ and $\hat{S}(z^{-1})$ exist. Note, however that, in the frequency range: $0 - 1000Hz$, the magnitude response and phase response match quite well.

From design aspect, Design 1 needs identification of the secondary path dynamics which may be of high order. If offline identification is not easy to carry out, Design 2 can be used since plant model is often available.

5 CONCLUSION

In this report, two designs of the adaptive feedforward compensation for vibration suppression based on IIR filter structure have been proposed. Simulation on a realistic open-source HDD benchmark problem showed that the proposed designs made the PES 3σ value smaller than the conventional FxLMS algorithm. The proposed designs are suitable for low frequency vibration suppression when

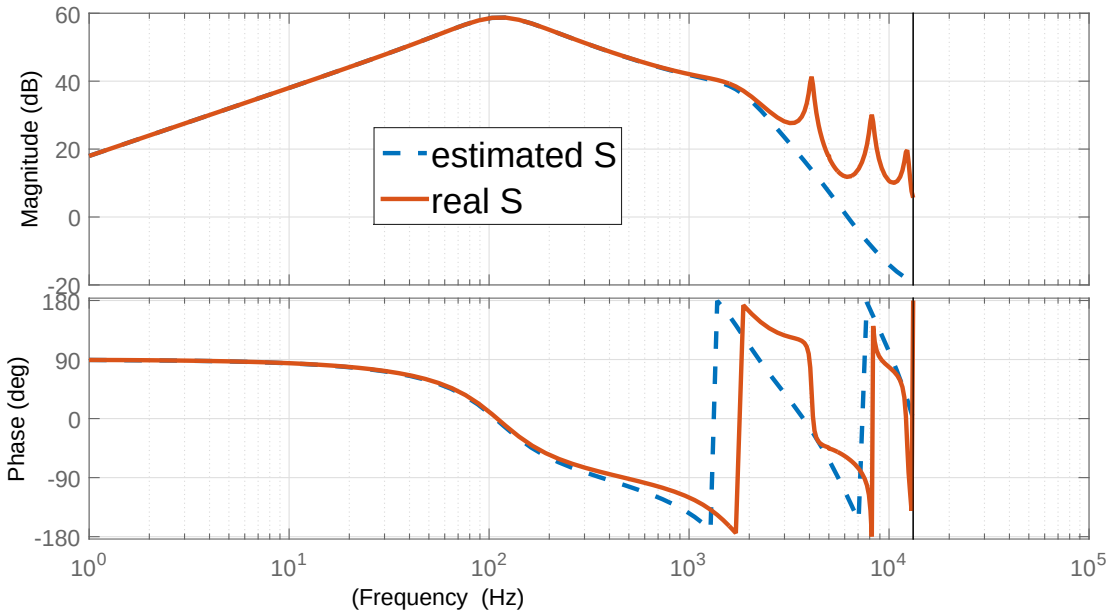

Figure 6: FREQUENCY RESPONSE OF $S(Z^{-1})$ AND $\hat{S}(Z^{-1})$

the vibration signal is available. Other ways of parameterizing the IIR filter is possible based on computational cost and complexity of the VTP. If the adaptive IIR needs to be of high order, the lattice parameterization [14] can be used for simple stability monitoring and the proposed structures are still applicable.

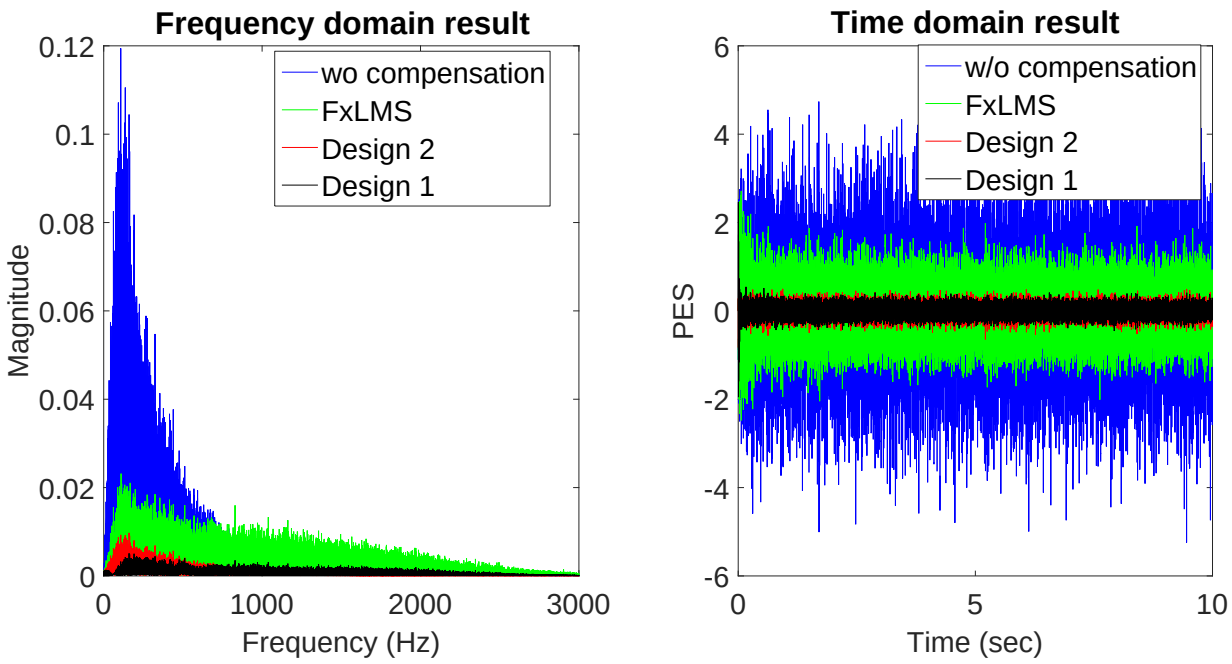

Figure 7: POWER SPECTRUM AND TIME SEQUENCE OF PES SIGNAL IN THREE CASES WITH PROPOSED DESIGN 1

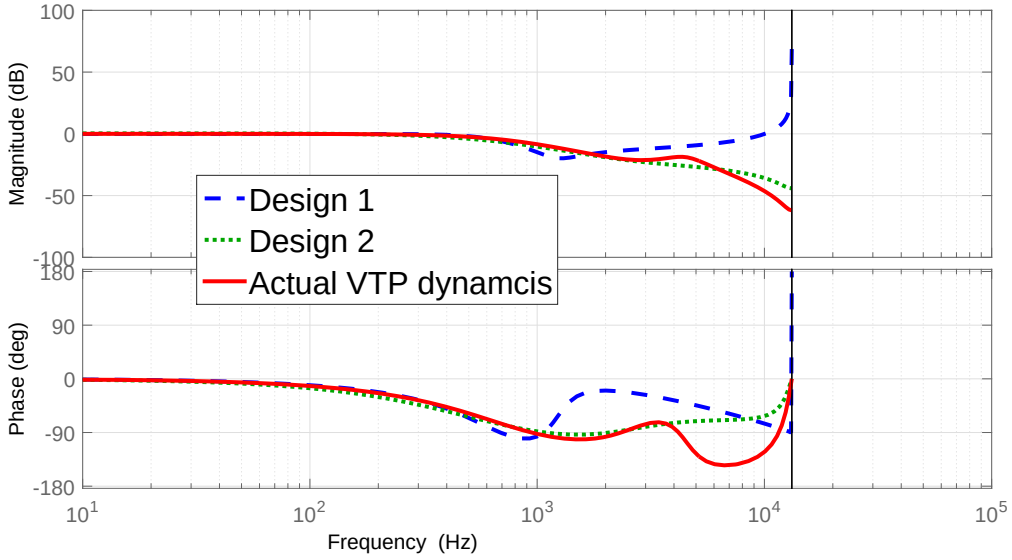

Figure 8: ACTUAL VTP DYNAMICS AND ADAPTIVE IIR AT STEADY STATE WITH DESIGN 1 AND 2

References

[1] K. J. Åström and B. Wittenmark. *Adaptive control*. Courier Corporation, 2013.

[2] E. Bjarnason. Analysis of the filtered-x lms algorithm. *Speech and Audio Processing, IEEE Transactions on*, 3(6):504–514, Nov 1995.

[3] X. Chen and M. Tomizuka. An indirect adaptive approach to reject multiple narrow-band disturbances in hard disk drives. In *proceedings of 2010 IFAC Symposium on Mechatronic Systems, IFAC*, pages 44–49, 2010.

[4] X. Chen and M. Tomizuka. An enhanced repetitive control algorithm using the structure of disturbance observer. In *Advanced Intelligent Mechatronics (AIM), 2012 IEEE/ASME International Conference on*, pages 490–495, July 2012.

[5] S. Dimolitsas. An adaptive {IIR} filter based on the hurwitz stability properties and a chebychev system function approximation. *Signal Processing*, 17(1):39 – 50, 1989.

[6] S. Elliott and P. Nelson. Active noise control. *Signal Processing Magazine, IEEE*, 10(4):12–35, Oct 1993.

[7] L. Eriksson, M. Allie, R. Greiner, et al. The selection and application of an iir adaptive filter for use in active sound attenuation. *Acoustics, Speech and Signal Processing, IEEE Transactions on*, 35(4):433–437, 1987.

[8] L. Eriksson, M. Allie, D. Melton, S. Popovich, and T. Laak. Fully adaptive generalized recursive control system for active acoustic attenuation. In *Acoustics, Speech, and Signal Processing, 1994. ICASSP-94., 1994 IEEE International Conference on*, volume 2, pages II–253. IEEE, 1994.

[9] M. Hirata. Nss benchmark problem of hard disk drive system, 2007.

[10] R. Jones, B. L. Olsen, and B. R. Mace. Comparison of convergence characteristics of adaptive iir and fir filters for active noise control in a duct. *Applied Acoustics*, 68(7):729–738, 2007.

[11] M. Kawafuku, K. Otsu, H. Hirai, and M. Kobayashi. High performance controller design of hdd based on precise modeling using differential iteration method. In *American Control Conference, 2003. Proceedings of the 2003*, volume 5, pages 4341–4346 vol.5, June 2003.

[12] I. D. Landau, R. Lozano, and M. M'Saad. *Adaptive Control*. Springer-Verlag New York, Inc., Secaucus, NJ, USA, 1998.

[13] R. Moses and D. Liu. Determining the closest stable polynomial to an unstable one. *Signal Processing, IEEE Transactions on*, 39(4):901–906, Apr 1991.

[14] P. Regalia. An improved lattice-based adaptive iir notch filter. *Signal Processing, IEEE Transactions on*, 39(9):2124–2128, Sep 1991.

[15] G. Stein. Respect the unstable. *Control Systems, IEEE*, 23(4):12–25, Aug 2003.

[16] K. Usui, M. Kisaka, A. Okuyama, and M. Nagashima. Reduction of external vibration in hard disk drives using adaptive feed-forward control with single shock sensor. In *Advanced Motion Control, 2006. 9th IEEE International Workshop on*, pages 138–143, 2006.

[17] S. Weerasooriya and D. Phan. Discrete-time lqg/ltr design and modeling of a disk drive actuator tracking servo system. *Industrial Electronics, IEEE Transactions on*, 42(3):240–247, Jun 1995.

[18] M. White and M. Tomizuka. Increased disturbance rejection in magnetic disk drives by acceleration feedforward control and parameter adaptation. *Control Engineering Practice*, 5(6):741 – 751, 1997.

[19] Q. Zheng and M. Tomizuka. A disturbance observer approach to detecting and rejecting narrow-band disturbances in hard disk drives. In *Advanced Motion Control, 2008. AMC '08. 10th IEEE International Workshop on*, pages 254–259, March 2008.